Published online 9 November 2017

Nucleic Acids Research, 2018, Vol. 46, No. 2 ***e8***
doi: 10.1093/nar/gkx1050

Fluorescently-tagged human eIF3 for single-molecule spectroscopy

Alex G. Johnson[1,2], Alexey N. Petrov[3], Gabriele Fuchs[4], Karim Majzoub[5], Rosslyn Grosely[2], Junhong Choi[2] and Joseph D. Puglisi[2,*]

[1]Department of Chemical and Systems Biology, Stanford University, Stanford, CA 94305, USA, [2]Department of Structural Biology, Stanford University, Stanford, CA 94305, USA, [3]Department of Biological Sciences, Auburn University, Auburn, AL 36849, USA, [4]The RNA Institute, Department of Biological Sciences, University of Albany, Albany, NY 12222, USA and [5]Department of Microbiology and Immunology, Stanford University, Stanford, CA 94305, USA

Received August 22, 2017; Revised September 29, 2017; Editorial Decision October 14, 2017; Accepted October 24, 2017

ABSTRACT

Human translation initiation relies on the combined activities of numerous ribosome-associated eukaryotic initiation factors (eIFs). The largest factor, eIF3, is an ∼800 kDa multiprotein complex that orchestrates a network of interactions with the small 40S ribosomal subunit, other eIFs, and mRNA, while participating in nearly every step of initiation. How these interactions take place during the time course of translation initiation remains unclear. Here, we describe a method for the expression and affinity purification of a fluorescently-tagged eIF3 from human cells. The tagged eIF3 dodecamer is structurally intact, functions in cell-based assays, and interacts with the HCV IRES mRNA and the 40S-IRES complex *in vitro*. By tracking the binding of single eIF3 molecules to the HCV IRES RNA with a zero-mode waveguides-based instrument, we show that eIF3 samples both wild-type IRES and an IRES that lacks the eIF3-binding region, and that the high-affinity eIF3–IRES interaction is largely determined by slow dissociation kinetics. The application of single-molecule methods to more complex systems involving eIF3 may unveil dynamics underlying mRNA selection and ribosome loading during human translation initiation.

INTRODUCTION

mRNA translation is a structurally and compositionally dynamic process. In eukaryotes, initiation is the most complex stage of translation, establishing the reading frame for protein synthesis and acting as an important input for post-transcriptional gene regulation (1–3). The complexity of initiation arises through the interplay of eukaryotic initiation factors (eIFs), the small 40S ribosomal subunit, and an mRNA. Initiation factors recruit the small 40S ribosomal subunit to the 5' methyl guanylate cap, guide it across the 5' untranslated region (5'UTR) to a start codon, and recruit the large 60S ribosomal subunit to form an elongation-competent 80S complex (1,3–6). The complete picture of how these interactions take place during the time course of initiation, and how these might be altered for regulation, remains unsettled. We have previously developed methods for the purification and fluorescent labelling of ribosomal subunits from yeast and human cells, and have used them to track ribosomal complexes in real time using a simple model of initiation that does not require initiation factors (7–9). Yet, revealing the more complex and biologically-relevant mechanisms of translation requires tracking the dynamic compositions of eIFs and their assembly pathways within pre-initiation complexes (PICs).

To study human translation initiation, we chose eIF3 as a target for specific fluorescent labelling, based on its multifaceted role in cellular and viral translation. eIF3 is the largest initiation factor with a total mass of ∼800 kDa. In mammals, it is composed of 12 non-identical subunits (eIF3a-i, k-m) and the loosely-bound eIF3j, which is more of an 'eIF3-associated factor' (10–13). By wrapping around the solvent side of the 40S ribosome, eIF3 extends the mRNA channel and mediates interactions with other eIFs and the auxiliary factor DHX29, interactions which have the potential to alter the conformation of the mRNA entry channel via eIF3j (14–18). The mammalian eIF3 structure is composed of a PCI/MPN (PCI: Proteosome cap, COP9 signalosome, eIF3; MPN: MprI-PadI N-terminal domain) octameric core of subunits (a, c, e, f, h, k, l and m) and peripheral subunits (b, d, g, i and j) (12,19,20). The octameric core forms a rigid five-lobed particle that is often described in anthropomorphic terms, and binds to the 40S subunit adjacent to the mRNA exit channel (Figure 1C) (10,12,20,21). The rigidity of the octamer has enabled extensive structural investigations, resulting most recently in a ∼6 Å reconstruc-

*To whom correspondence should be addressed. Tel: +1 650 498 4397; Fax: +1 650 723 8464; Email: puglisi@stanford.edu

© The Author(s) 2017. Published by Oxford University Press on behalf of Nucleic Acids Research.
This is an Open Access article distributed under the terms of the Creative Commons Attribution License (http://creativecommons.org/licenses/by-nc/4.0/), which permits non-commercial re-use, distribution, and reproduction in any medium, provided the original work is properly cited. For commercial re-use, please contact journals.permissions@oup.com

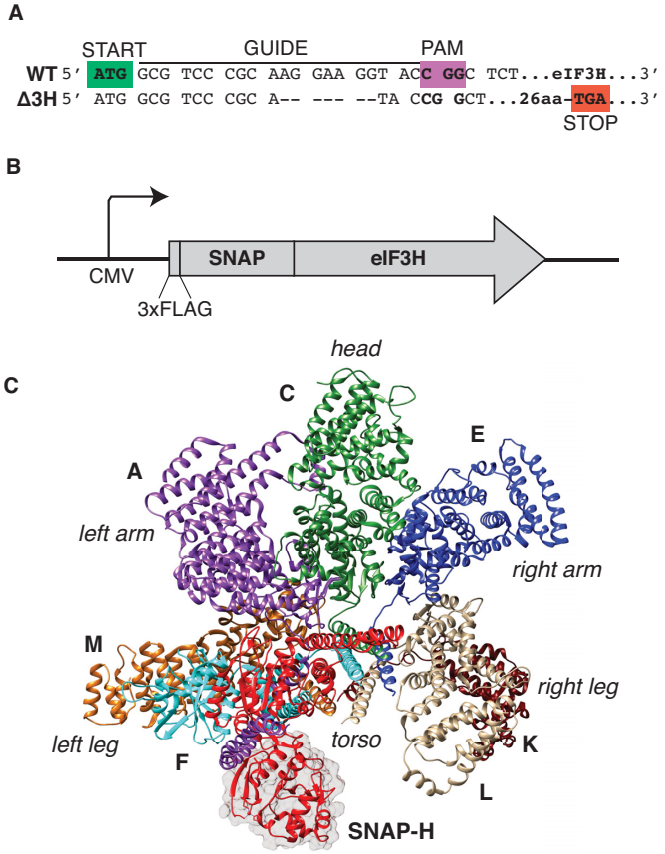

Figure 1. Human eIF3 labeling strategy. (**A**) Isolation of a eIF3H knockout (Δ3H) Hap1 strain using CRISPR/Cas9-mediated genomic disruption. (**B**) Genetic complementation by stable expression of 3xFLAG-SNAP–eIF3H. (**C**) Structural model of the mammalian eIF3 octameric core with an N-terminally labeled SNAP–eIF3h. The structure is annotated to indicate anatomical positions and the location of subunits of the PCI/MPN octamer. The image was created in UCSF Chimera using the model of the eIF3 octamer in the context of the 43S pre-initiation complex (PDB 5A5T) and a benzylated SNAP tag (PDB 3L00, highlighted by a grey surface) (79,80).

tion in the context of the 43S PIC by cryo-EM (20,22–25). In contrast, peripheral subunits form densities at lower resolution, likely due to the flexibility of the 43S PIC assembly (24). Structural investigations have begun elucidating snapshots of the peripheral subunits in the late 48S PIC, where they may undergo a series of structural rearrangements (26). These results underscore the dynamic nature of eIF3 conformation, but when and how eIF3 interacts with mRNA, other eIFs, and the ribosome in the course of translation initiation is unresolved.

In special cases, eIF3 makes specific contacts with RNA structures within cellular and viral RNAs. Perhaps the best-studied example is the high-affinity interaction between eIF3 and a domain within the type 3 Hepatitis C virus (HCV) internal ribosome entry site (IRES) RNA (27–29). By binding within domain IIIb and the IIIabc junction of the IRES, eIF3 forms an unusual ternary complex with the 40S-IRES wherein the octameric core is occluded from its canonical 43S PIC binding position (25). Acting through multiple subunits, this interaction enables eIF3 to mediate functions that drive translation initiation from the IRES, and the eIF3-binding site is thus functionally crucial and used not only by type 3 IRESs, but also by diverse picornavirus IRESs (30–34). Separately, eIF3 binds the 5′ cap and RNA structures of select cellular mRNAs, and these interactions serve to up- and downregulate the synthesis of proteins important in cancer (35,36). How these specialized interactions interface with the function of eIF3 in general translation remains largely unexplored.

Here, we describe a strategy to incorporate a stable, fluorescent label into eIF3 for single-molecule studies. We used targeted genome engineering to delete a core eIF3 subunit in a human cell line and replaced it with a version that can be fluorescently labeled and affinity purified. While most methods for the purification of human eIF3 require multi-step procedures for either native or recombinant purification, we devised a simple affinity-based method for purification of the native complex such that it is fully intact and detectable by its fluorescence. This method provided an eIF3 that can be tracked in single-molecule fluorescence assays, revealing the kinetics behind discrimination of a domain within the HCV IRES RNA.

MATERIALS AND METHODS

Cell growth and genetic manipulations

Hap1 cells were grown at 37°C, 5% CO_2 in Iscove's modified Dulbecco's medium (IMDM; HyClone) supplemented with 10% FBS, 2 mM L-glutamine, and 1X penicillin/streptomycin. The DNA oligonucleotides F1 and R1 were annealed and ligated into the pX458 vector (a gift from Feng Zhang, Addgene plasmid #48138) for CRISPR/Cas9 mutagenesis of the eIF3H locus at exon 1 (37). All DNA oligonucleotide sequences are listed in Supplementary Table S1. The CRISPR/Cas9 plasmid was transfected into Hap1 cells with Lipofectamine 3000 (Thermo Fisher Scientific), and individual GFP-positive cells were sorted into wells of a 96-well culture plate. Clones were recovered over several weeks and KO cells were identified by screening clones by western blotting for eIF3h. Candidate eIF3H KO clones were further verified by extracting genomic DNA with the QIAamp DNA mini kit (QIAGEN), PCR amplifying around exon 1 with primers F2 and R2 using Phusion DNA polymerase (NEB), and then sequencing the PCR amplicon with the F2 primer (Supplementary Figure S1).

To create an N-terminal SNAP-tagged eIF3H expression construct, the eIF3H ORF was PCR amplified from a FLAG-HA-eIF3S3 vector (a gift from Wade Harper, Addgene plasmid #22545) (38). The PCR primers F3 and R3 were used for amplification and the amplicon was inserted into the pSNAPf plasmid (NEB) at the BamHI and the XhoI sites. The SNAP–eIF3H fusion was then amplified with primers F4 and R4 to add N-terminal 6xHis tag and TEV site and cloned into pENTR/D-TOPO entry vector (Thermo Fisher Scientific). The 3xFLAG-tagged SNAP–eIF3H was made by re-amplifying this entry vector with the forward primer F5 and R5. The SNAP–eIF3H sequence was then transferred to the pLenti CMV Puro DEST plasmid (a gift of Eric Campeau, Addgene plasmid #17452) using LR clonase II (Thermo Fisher Scien-

tific) (39). The SNAP–eIF3H lentiviral vector was packaged in HEK293FT cells, and packaged lentivirus was transduced into Hap1 cells followed by selection with 1 μg/ml puromycin.

Proliferation and luciferase assays

MTT proliferation assays were carried out with the Vybrant Assay Kit (Life Technologies), following the manufacturer's protocol. Hap1 cells were seeded in 96-well culture plates at 10 000 cells per well with 10 replicates per strain in phenol red-free IMDM media. Cells were assayed for growth over the course of 5 days. Absorbance values at 570 nm were determined using an Epoch (BioTek) plate reader and values were normalized to background (media only).

The dual-luciferase reporter assay kit (Promega) was used to measure the Renilla (cap-dependent) and firefly (cap-independent) luciferase levels using IRES reporter constructs for the Poliovirus, Encephalomyocarditis virus, Hepatitis C virus, and Cricket Paralysis virus IGR (all gifts from Peter Sarnow). Cells were seeded in 24-well culture plates at 50 000 cells/well, grown for 24 h, and then each well was transfected with 1 μg/well plasmid DNA using Lipofectamine 3000. After an additional 24 h of growth, cells were lysed and assayed for luciferase activity using a GloMax 20/20 Single-Tube luminometer, using 10 second integrations for each reading. Experiments were performed with five biological replicates of each strain/plasmid.

Immunoblotting

Cell lysates were prepared with 1× lysis buffer from the dual-luciferase kit (Promega) and centrifuged at 15 000 rcf for 10 min in a Eppendorf 5418 microcentrifuge to remove insoluble material. The protein concentration of lysates was determined with a Bradford assay (BioRad) and the protein concentration from multiple lysates was normalized prior to loading on an SDS-PAGE in Laemmli sample buffer (5 μg per lane). Proteins were separated by 4–20% SDS-PAGE (BioRad) and transferred to PVDF membranes by standard procedures. Membranes were incubated with antibodies in 5% skim milk in TBST. All antibodies used are listed in Supplementary Table S2. HRP-conjugated antibodies were detected with SuperSignal West Dura Extended Duration Substrate (Thermo Scientific) using a ChemiDoc Touch Imaging System (BioRad). When blots were re-probed blots with a loading control, membranes were incubated for an hour in block containing 0.02% sodium azide to inactivate HRP secondary antibodies prior to incubation with new primary antibodies. Full western blots from cell lysate of Hap1 cell lines are shown in Supplementary Figure S2.

SNAP–eIF3 purification and characterization

3xFLAG-SNAP–eIF3 expressing eIF3H KO cells were grown to 80–90% confluence in 10–20 15-cm plates, dissociated with trypsin, pelleted, washed, and harvested in PBS. Cell pellets (∼1–2 g of cell mass) were either first flash-frozen or immediately lysed by incubation in 5–10 ml lysis buffer (50 mM Tris–HCl pH 7.5, 150 mM NaCl, 0.5% Triton-X 100, 1 mM EDTA, 10% glycerol) with cOmplete protease inhibitor (Sigma-Aldrich) and Pierce phosphatase inhibitor (ThermoFisher) tablets. Lysates were clarified by centrifugation at 12 000 rcf for 15 min in the F21 rotor (ThermoFisher) and passaged through a 0.22 μm syringe filter. The clarified lysate was mixed with 5 nmol SNAP dye substrate (NEB) and incubated with anti-FLAG M2 magnetic beads (Sigma-Aldrich) for 4–12 h at 4°C, followed by five washes with Tris-buffered saline pH 7.5 (TBS), following the manufacturer's protocol. Beads were washed twice with high-salt (500 mM NaCl) TBS to ensure the removal of nucleic acids and ribosomal complexes. SNAP–eIF3 was eluted with two volumes of TBS buffer containing 100 μg/ml 3xFLAG peptide (Sigma-Aldrich), followed by concentration and washing with TBS (containing 1 mM DTT) with a 100 kDa MWCO concentrator (Millipore). Fractions from the purification were analysed by SDS-PAGE, and concentrated sample was analysed by non-denaturing 5% acrylamide PAGE in TBE buffer (Supplementary Figure S3 and Figure 3). Concentrated samples were frozen in liquid nitrogen, and stored at –80°C. PAGE gels were imaged for fluorescence using a Typhoon Imaging System (GE Healthcare), and then stained with either SimplyBlue (ThermoFisher) or Coomassie R-250, destained, and imaged with a scanner or ChemiDoc imaging system. We analysed SNAP–eIF3 samples alongside HeLa eIF3 by western blots, to ensure that all subunits were full-length and present at roughly equal stoichiometry (Figure 3B). A single preparation typically yielded ∼50–100 μl of ∼500 nM SNAP–eIF3. SNAP–eIF3 concentration was measured by two methods: SNAP dye fluorescence by absorbance with a nanodrop spectrophotometer and a standard curve of labelled recombinant SNAP (Supplementary Figure S3). Both methods gave similar measurements, but the standard curve was more sensitive at lower concentrations of SNAP–eIF3.

Recombinant 6xHis-SNAP protein was expressed in and purified from *Escherichia coli* BL21 (DE3) using the pFLAG-SNAP-MCS-HIStag expression plasmid, which was a gift from Anupam Chakravarty. Two liters of cells were grown at 37°C in LB containing kanamycin (50 μg/ml) to an OD_{600} of 0.5. Protein expression was induced by the addition of 1 mM IPTG and cultures were incubated overnight at 17°C. Cells were lysed by sonication in lysis buffer (20 mM Tris-HCl pH 7.5, 150 mM NaCl, 10 mM imidazole, 5 mM BME, 10% glycerol) and the lysate was clarified by centrifugation at 38 000 rcf in the F21 rotor and filtration through a 0.22 μm syringe filter. 6xHis-SNAP was purified from the lysate by incubating with 3 ml Ni-NTA agarose (QIAGEN), loading onto a gravity-flow column, washing with high-salt (1 M NaCl) buffer, and eluting with buffer containing 250 mM imidazole. Eluted fractions containing 6xHis-SNAP were dialyzed into gel filtration buffer (20 mM HEPES–KOH pH 7.5, 150 mM KCl, 10% glycerol, 1 mM DTT) overnight with a 10 kDa MWCO cassette (ThermoFisher), and then purified by size-exclusion chromatography with a Superdex 200 10/300. Column fractions containing monomeric SNAP were combined and labelled with a sub-stoichiometric concentration of SNAP-Surface 649 substrate. Non-reacted dye was removed by buffer exchange with a 10-DG column (BioRad), labelled protein was concentrated with a 10 kDa MWCO concentrator (Mil-

lipore), and the concentration of SNAP dye was determined by nanodrop. The labelled recombinant SNAP protein was used to make a standard curve for determining the concentration of SNAP–eIF3 by fluorescence imaging of an SDS-PAGE gel with a Typhoon Imaging System (Supplementary Figure S3).

HeLa eIF3 and Hap1 ribosome purification

HeLa cell eIF3 was purified as described, along with advice from Chris Fraser (UC Davis) (18,40). The postnuclear cell extract used for purification was a kind gift from Robert Tijan (UC Berkeley). Human 40S ribosomes were purified from Hap1 cells by a 10–30% sucrose gradient, after splitting 80S ribosomes with the puromycin method (8). Both wild-type and eS25-SNAP 40S ribosomal subunits were purified for these studies, and in the latter case the ribosomes were labelled with the SNAP-Surface 549 dye substrate for Cy3-like fluorescence detection, as previously reported (8).

RNA transcription and labelling

HCV IRES transcription plasmids were modified from a previously described HCV IRES transcription construct in pUC19 that was designed for the annealing of fluorescent and biotinylated DNA oligonucleotides (8). The F6 and R6 primers were used to amplify the HCV IRES, which was subsequently inserted back into pUC19 at HindIII and XbaI sites to create a new wild-type construct for segmental labelling within domain II (Supplementary Figure S4). The dII-mid transcription construct was made by amplifying from the wild-type construct with primers F7 and R6, and inserted into HindIII and XbaI sites (32). The del-IIIabc transcription construct was made by amplifying from the wild-type construct with primers F6 and R7, and inserted into HindIII and NheI sites (the latter within the domain III sequence of the HCV IRES) (32). Transcription plasmids were linearized by NarI and *in vitro* transcribed with T7 polymerase as described (8). When preparing transcripts for segmental labelling, a two-fold excess of GMP to GTP was used to ensure that the majority of transcripts contain a 5' monophosphate (41). Transcribed RNA was purified and concentrated as described (8). Select RNAs were segmentally labelled at their 5' end with T4 RNA ligase (NEB) and a synthetic CCUGUG AGGAACUACU RNA oligonucleotides, where the bold U has been base-modified with Cy3 (TriLink) (Supplementary Figure S3) (41). The ligation reaction was carried out overnight at 25°C, extracted with acidic phenol-chloroform-isoamylalcohol (25:24:1) and chloroform, and precipitated with ethanol and sodium acetate. Excess RNA oligo was removed from the ligated product with mini P6 gel filtration columns (BioRad). This labelling strategy places a fluorescent dye within the flexible multinucleotide bulge of domain IIa, with dye exposed to solvent in the free IRES form or while bound as a 40S- or 80S-IRES complex (42–44).

RNA was refolded prior to each experiment as described (8). When performing single-molecule experiments, refolding took place in the presence of a two-fold excess of the biotinylated DNA oligonucleotides (biotin-CTCTCTCGCC GGGCCTTTCTTTATG), which is complementary to an unstructured sequence at the 3' end of each RNA. This strategy ensured that only full-length RNAs are biotinylated at their 3' end for immobilization on neutravidin-coated surfaces.

Composite gel shift assay

Complexes of the HCV IRES, 40S ribosomal subunit, and eIF3 were resolved using acrylamide/agarose composite gels (45,46). The composite gels were composed of 2.75% acrylamide (37.5:1), 0.5% Nusieve GTG agarose, 2.5% glycerol, 0.5 mM DTT, 0.1% TEMED and 0.1% APS, and handcast with 1.5 mm Mini-PROTEAN plates (BioRad). Gels were cast and run in a buffer of 25 mM Tris-Acetate (pH 7.0), 6 mM $KOAc_2$ and 2 mM $MgOAc_2$. Agarose was rapidly solidified by cooling gels at 4°C for 10 minutes immediately after initiating polymerization, and then brought to room temperature for an hour to complete polymerization (46).

Complexes were formed by incubating Cy3-labeled HCV IRES with either or both dark 40S ribosomal subunits or SNAP-649-eIF3 at 30°C for 10 min. Samples were then mixed with 10× loading dye (50% sucrose with bromophenol blue), loaded onto a pre-run gel, and run for one hour at 100 V. The fluorescence of the Cy3-IRES and SNAP-649 was detected using a Typhoon scanner, and the images were analysed in ImageJ.

Single-molecule spectroscopy

Immediately before each experiment, IRES RNAs were re-folded and annealed with biotinylated-DNA oligonucleotides (8). In static experiments using total internal reflection fluorescence microscopy (TIRFM), ternary complexes of Cy3-like labeled 40S ribosomal subunit (SNAP(549)-40S), biotinylated IRES, and Cy5-like eIF3 (SNAP(649)-eIF3) were formed at a 2:1:2 stoichiometry (50 nM IRES final) by incubation for 15 min at 30°C in 30 mM HEPES-KOH (pH 7.4), 100 mM KCl, and 5 mM $MgCl_2$ (Recon-Cl buffer). Complexes were immobilized by adding 20 μl of 50 pM complexes (by IRES concentration) in the channels of neutravidin-covered quartz slides for 5 min. Unbound complexes were washed from the slide with Recon-Cl buffer supplemented with 2.5 mM trolox (TSY), 2.5 mM protocatechuic acid (PCA), and 0.06 U/μl protocatechuate-3,4-dioxygenase (PCD) (47). Complexes were then imaged with 532 and 647 nm lasers, using a prism-based TIRF setup described previously (47). Short (50 frame) and long (5000 frame) movies were acquired at 10 frames per second (fps), and colocalized molecules were identified using custom MATLAB scripts (MathWorks).

For delivery experiments in zero-mode waveguides (ZMWs), all imaging was performed with a modified DNA sequencer from Pacific Bioscience (48). For immobilization, Cy3- and biotin-labelled RNAs were first diluted to 100–500 pM RNA (by Cy3 concentration) in 30 mM HEPES–KOH (pH 7.4), 100 mM KOAc and 5 mM $Mg(OAc)_2$ (Recon buffer). A 20 μl sample of diluted RNA was then incubated on the neutravidin-coated surface of ZMW chips for 5 min, and unbound RNA was removed by multiple

washes with Recon buffer. Prior to imaging, the chip surfaces were washed and left in 20 μl Recon buffer supplemented with TSY, PCA, and PCD (as described above). A 20 μl sample containing 1 nM of SNAP(649)-eIF3 was delivered to the chip surface at the beginning of acquisition. Movies were acquired at 10 fps for 15 minutes using the 0.30 $\mu W/\mu m^2$ 532 nm and 0.24 $\mu W/\mu m^2$ 650 nm illumination settings. ZMW movies were analysed using custom MATLAB scripts in order to extract kinetic parameters. The complete fit results are summarized in Supplementary Tables S3 and S4.

RESULTS

Choice of labeling strategy

Human eIF3 is typically obtained by native purification from salt-washed ribosomes or reconstituted via individual subunit expression in *E. coli* (20,40). Both strategies have their advantages and disadvantages. The native method requires hundreds of litres of cultured mammalian cells and provides an intact eIF3 with post-translational modifications; whereas the recombinant method enables subunit mutagenesis, but provides an eIF3 with certain subunits partially cleaved (20,33). Given the low material quantities required for single-molecule analysis, we sought a method for a simple affinity-based purification of eIF3 that is fully intact.

We began by identifying a subunit of eIF3 in which we could incorporate a stable, non-disruptive affinity-handle for human eIF3. For genetic manipulations, we first considered non-essential subunits, previously identified by yeast genetics. In the six-subunit eIF3 of budding yeast, most subunits (a, b, c, g, i) are essential, while the sub-stoichiometrically bound j-subunit is non-essential (49). However, in the 11-subunit eIF3 of fission yeast, the e, d, and h subunits are non-essential, but this eIF3 was proposed to be compositionally distinct from mammalian eIF3, forming two separate complexes (50,51). *In vitro* reconstitution studies have suggested that subunits a, b, c, e, f and h constitute a 'functional core' of human eIF3, while a partially overlapping group of subunits (a, c, e, f, h, k, l and m) form a structurally stable octameric core (20,52). Surprisingly, the h-subunit, a component of the structural and functional core, is non-essential for growth in *Neurospora crassa*, a species with a human-like set of 13-subunits (53). Additional RNAi studies in fruit flies have suggested that reductions in the h-subunit causes minimal growth defects, and this was also recently confirmed in HeLa and HEK293T cells (13,54,55). We thus focus here on eIF3h for tagging, as it appeared to be non-essential for cell growth, yet still a core structural component of eIF3 with no known intrinsic RNA-binding activity (20,52).

eIF3H mutagenesis and genetic complementation

The human haploid (Hap1) cell line was chosen for modification as it enables facile genetic manipulation of non-essential genes, and we have used it previously to label and purify human ribosomes (8). Hap1 cells were genetically modified with a construct encoding *S. pyogenes* Cas9 protein and guide strand construct targeting exon 1 of eIF3H. Knockouts (KOs) were identified by screening FACS-sorted single-cell clones with western blots for eIF3h, followed by sequencing at the eIF3H genomic locus. We identified a clone with a seven nucleotide deletion that causes a frameshift leading to a pre-mature stop codon in exon 1 (Figure 1A and Supplementary Figure S3) (56). Following clone isolation, the eIF3H KO growth defect was apparent, as the first mutants to arise after CRISPR/Cas9 mutagenesis had in-frame insertions and low but detectable eIF3h levels (not shown).

After isolation of the eIF3H KO (Δ3H), we designed an eIF3H expression construct containing both an affinity and fluorescent tag (Figure 1B). For specific fluorescent labelling, we used the mutant O^6-alkylguanine DNA alkyltransferase tag (SNAP-tag), as it enables high-efficiency labelling with a versatile series of substrates. The N-terminus was chosen for modification as a previous study of recombinant eIF3 had shown the effective incorporation of an N-terminal MBP tag, and we reasoned that we could prepare an eIF3 similarly modified at this position (Figure 1C) (23). To achieve high levels of stable expression, 3xFLAG-SNAP–eIF3H (SNAP-3H) was integrated into Hap1 strains by lentiviral transduction and expressed under the control of a CMV promoter. SNAP–eIF3H expression was confirmed by immunoblotting with antibodies against eIF3h and FLAG that showed the appearance of a ∼60 kDa protein corresponding to the combined molecular weight of eIF3h (∼40 kDa) and SNAP (∼20 kDa) (Figure 2A). SNAP–eIF3h expresses at near wild-type levels via comparison with the loading control (nuclear matrix protein p84), and we further noted that SNAP–eIF3h overexpression diminishes endogenous levels of eIF3h in wild-type cells (Figure 2A). During the characterization of the eIF3H KO strain, we noticed that the subunits k and l of the 'right leg' of the eIF3 octameric core were at reduced levels in cell lysate, a finding that is consistent with a RNAi knockdown of eIF3H in HeLa cells and the results from immunoprecipitation experiments in HEK293T cells (13,55). This observation provided a convenient read-out for the structural stability of eIF3 in the SNAP–eIF3h expressing Δ3H cells (SNAP-3H addback). Indeed, upon expression of SNAP–eIF3 in the Δ3H cells (SNAP-3H addback) we observed restoration of wild-type levels of the subunits k and l, suggesting that SNAP–eIF3h functionally substitutes for the wild-type subunit (Figure 2A and Supplementary Figure S2).

We next used cell proliferation assays to test whether the SNAP-3H addback cells display similar growth characteristics to wild-type cells. We observed the expected growth defect of the Δ3H strain, while the SNAP-3H addback strain restored proliferation to near wild-type levels for each day over a 5-day period (Figure 2C). These results suggest that SNAP–eIF3h effectively substitutes for wild-type eIF3h in general cellular translation, yet we further probed SNAP–eIF3h functionality in cap-dependent and IRES-mediated translation using a set of dual-luciferase reporter constructs. By assaying relative translation efficiency, we noticed that the Δ3H cell line has a reduction in the ratio of cap-independent to cap-dependent translation of poliovirus (PV) and encephalomyocarditis (EMCV) IRES reporters, but no alterations for HCV and CrPV IGR IRES reporters

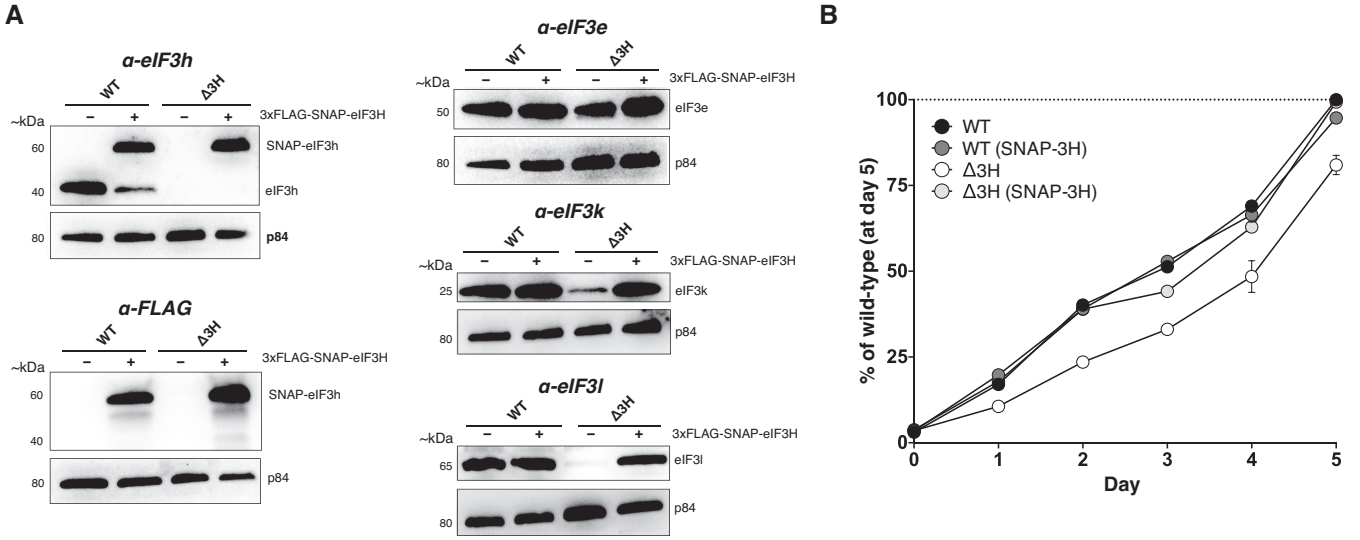

Figure 2. SNAP–eIF3H expression in the eIF3H KO restores wild-type eIF3 structure and function. (**A**) Western blots of wild-type (WT) and eIF3H KO (Δ3H) Hap1 cells +/– stable expression of 3xFLAG-SNAP–eIF3H (SNAP-3H). Blots were probed with antibodies against eIF3h, FLAG, eIF3e, eIF3k, and eIF3l, and each blot was re-probed with an antibody against p84 (loading control). (**B**) MTT proliferation assay over a five-day time course. Values are presented as the percent of absorbance at 570 nm of the wild-type average on day 5, and error bars represent the 95% confidence intervals of 10 biological replicates.

(Supplementary Figure S5). Importantly, the SNAP-3H addback restored the luciferase ratio to near wild-type levels for each reporter, further validating that the addback functionally restored translation changes in the Δ3H cell line.

SNAP–eIF3 purification and validation

Since eIF3h is a stably-associated subunit and the SNAP-3H addback cell line displays wild-type levels of all eIF3 subunits, we reasoned that affinity purification of SNAP-3h would yield a full and intact SNAP–eIF3 complex. The addback cell line was expanded in culture, cells were harvested and lysed. A SNAP dye substrate was added to clarified lysate for labelling, and this mixture was incubated with anti-FLAG magnetic beads (Figure 3A). By directly labelling the SNAP-tag in lysate, we were able to readily track SNAP–eIF3h through each purification and elution step (Supplementary Figure S3). While our initial purification method utilized a polyhistidine-tag, we changed the construct to a 3xFLAG-tag to optimize purity and yield. In parallel, SNAP–eIF3 was purified from a crude ribosome pellet isolated through a low-salt sucrose cushion, but this method resulted in a substantial decrease in yield and was not further pursued (not shown). The isolated SNAP–eIF3 from the bead-based purification contains each full-length eIF3 subunit at near-stoichiometric levels compared to that of an eIF3 purified from HeLa cell post-nuclear lysate (HeLa eIF3), using a previously-described method (40) (Figure 3B). Additionally, SNAP–eIF3 migrates at a similar apparent molecular weight to HeLa eIF3 on a non-denaturing 5% acrylamide gel, appearing as a distinct fluorescent species, indicating that the tagged complex is structurally intact (Figure 3C).

In vitro binding assays with the HCV IRES and 40S ribosome

To test the functionality of tagged eIF3 *in vitro*, we investigated the binding of eIF3 to the HCV IRES RNA and the 40S ribosomal subunit using a composite gel shift assay. We first assembled SNAP(649)-eIF3 with Cy3-labelled HCV IRES with or without unlabelled human 40S ribosomal subunits, resolved complexes on an acrylamide/agarose composite gel, and imaged the gels for fluorescence arising from eIF3 and/or the IRES. Compared to the high-affinity 40S-IRES complex (K_d = ~2 nM), eIF3 is known to form a weaker but still specific interaction with the HCV IRES (K_d = ~35 nM), and only modestly increases the affinity of the 40S-IRES complex (30,32). Consistent with this affinity, a binary complex of SNAP–eIF3 and the IRES co-localize on a composite gel, but does not form a tight band like that of the 40S-IRES complex (Figure 4A). Yet when all three components are mixed together, a distinct higher apparent molecular weight band appears showing tight co-localization of labelled SNAP–eIF3 and the HCV IRES.

To assess whether similar complexes containing SNAP–eIF3 can be detected as single molecules on a surface, we next formed ternary complexes of biotinylated HCV IRES, SNAP(549)-40S and SNAP(649)-eIF3. Complexes were immobilized on the neutravidin-coated surface of a TIRFM slide and illuminated with 532- and 647-nm lasers. Under these conditions, green and red fluorescence appear when SNAP(549)-40S or SNAP(649)-eIF3 is stably bound to immobilized IRES, respectively. In addition to isolated green and red fluorescence, we observe co-localized fluorescence indicating the formation of 40S–IRES–eIF3 ternary complexes (Figure 4B-C). When illuminating solely with the 532-nm laser, we observed no fluorescence resonance energy transfer (FRET) between the labels on eIF3h and eS25 as expected, since location of these labels is greater than 10 nm apart (57). Since these experiments were performed un-

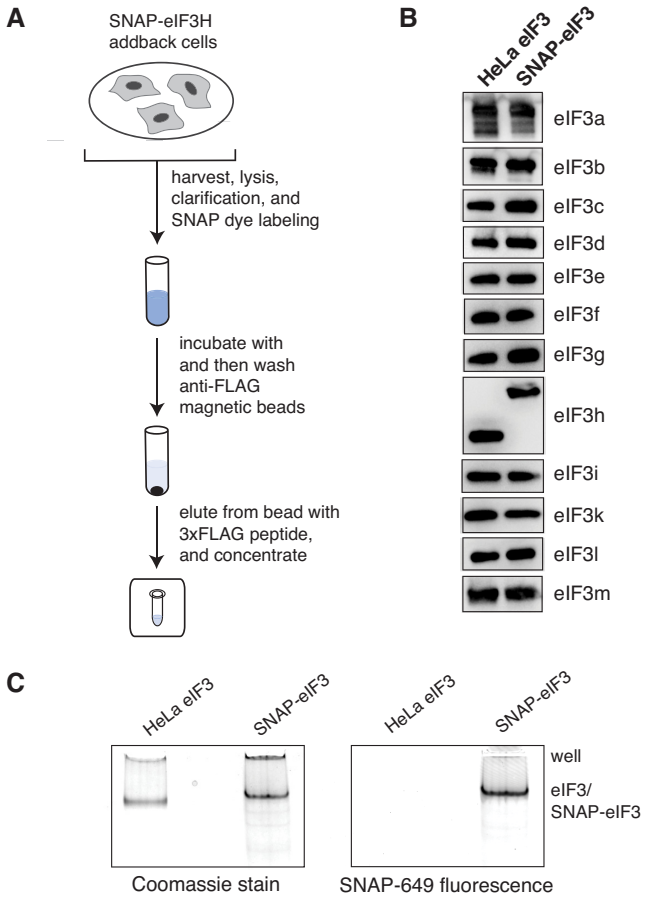

Figure 3. Affinity-based purification of SNAP–eIF3 from addback cells. (**A**) SNAP–eIF3 purification scheme using anti-FLAG magnetic beads. (**B**) Western blots of HeLa eIF3 and SNAP–eIF3 samples showing all subunits of the eIF3 dodecamer at equal stoichiometry. Samples were loaded at roughly equal amounts, using concentrations determined by absorbance at 280 and 655 nm for HeLa eIF3 and SNAP–eIF3, respectively. (**C**) Non-denaturing 5% acrylamide PAGE of HeLa eIF3 and SNAP–eIF3 samples.

der static conditions where the images were acquired minutes after immobilization, these fluorescent molecules represent very long-lived complexes. Individual green and red fluorescent molecules may reflect stable binary complexes or ternary complexes where either the 40S ribosomal subunit or eIF3 is unlabelled or has undergone photobleaching prior to image acquisition. Thus, real-time methods to monitor eIF3 binding to ribosomes are required to parse the true eIF3–IRES–40S subunit interaction kinetics.

Real-time imaging of eIF3 binding to the HCV IRES in ZMWs

The binding of eIF3 to type 3 HCV-like IRESs has been well-defined by equilibrium methods. eIF3 specifically interacts with the apical region of domain III of type III IRESs, and deletions or mutations of this region interfere with eIF3 binding and 80S-IRES formation (30–32,58). To test whether SNAP–eIF3 maintains this specificity in binding kinetics to the HCV IRES, we transcribed and fluorescently labelled wild-type and mutant IRES RNAs for immobilization in zero-mode waveguides (ZMWs) (Figure 5A and Supplementary Figure S4). Our mutant IRES RNAs were designed from previously studied deletions that both still bind the 40S ribosomal subunit with high-affinity: domain II-mid (dII-mid) that lacks the apical region of domain II, and domain IIIabc junction deletion (del-IIIabc) wherein domain IIIa-c is replaced by a small hairpin (Figure 4B) (32). Given that del-IIIabc lacks the major eIF3 binding region, SNAP–eIF3 is expected to display altered kinetics to this RNA, but near wild-type binding kinetics to the dII-mid IRES, as domain III is fully intact in this construct. The dII-mid mutant thus serves as a control to ensure that the removal of RNA segments outside of the IIIabc junction does not perturb eIF3 binding kinetics. The IRES RNAs were immobilized in separate ZMW chips, such that each eIF3 delivery experiment occurred sequentially to unique chips rather than in parallel on a single chip.

Upon delivery of SNAP(649)-eIF3 to Cy3-labeled HCV IRES RNAs immobilized in ZMW wells, we observed multiple bursts of red fluorescence (Figure 5C). To score for eIF3 binding events to single RNAs, immobilization took place at concentrations that favour single RNA molecules per ZMW according to Poisson statistics. Only ZMW wells with fluorescent traces demonstrating a single-step photobleaching event of Cy3 fluorescence were analysed for eIF3 binding events. As expected, we observe no anti-correlated fluorescent behaviour that would indicate FRET between the label at IRES domain II and eIF3h, since the N-terminus of eIF3h is distal from the major IRES interacting subunits eIF3a and c (33). The time between reagent delivery and SNAP(649)-eIF3 binding events (and between each subsequent binding event after SNAP(649)-eIF3 dissociation) were used to determine arrival lifetimes, while residence lifetimes are equivalent to the duration of each binding event.

For all examined RNAs, arrival and residence times are best described by double exponential functions. eIF3 binds to the wild-type RNAs with modestly faster kinetics than to either mutant IRES, although this difference is not accounted for by a large change in the fast arrival phase (Figure 5D and Supplementary Table S3). In contrast, we observe a distribution composed of fast (~0.3–0.5 s^{-1}) and slow (~0.03 s^{-1}) off-rates for wild-type and dII-mid IRES RNAs, while dwell times on the del-IIIabc IRES are notably shorter, displaying increased off-rates of ~1.7 and ~0.12 sec^{-1} for fast and slow populations, respectively (Figure 5D and Supplementary Table S4). Our kinetic data thus agree with the known specificity between eIF3 and the apical region of domain III, and indicate that it arises from a relatively long residence time.

DISCUSSION

The structural and functional complexity of eIF3 makes it a challenging target for labeling strategies. The absence of a direct relationship between the 'core' subunits present in budding yeast with those that constitute the structural and functional cores of the mammalian complex, created a dilemma in choosing which core subunit to modify. The finding that eIF3h, an MPN subunit of the eIF3 PCI/MPN octamer, is non-essential for growth of human cells suggests that translation initiation is elastic to perturbations in

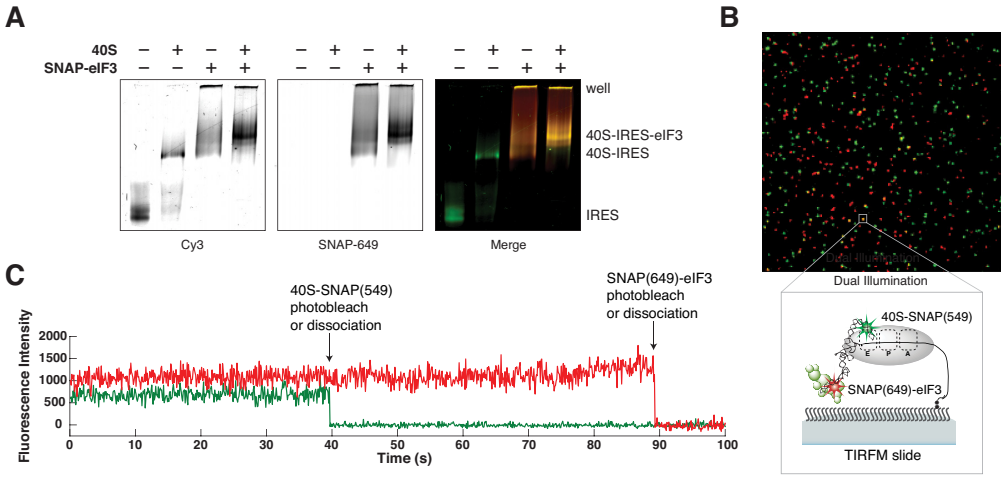

Figure 4. SNAP–eIF3 interacts with the HCV IRES and 40S ribosomal subunit *in vitro*. (**A**) Acrylamide/agarose composite gel of SNAP(649)-eIF3 and unlabeled 40S ribosomal subunit binding to Cy3-labeled HCV IRES. (**B**) TIRF view-field of IRES immobilized 40S-SNAP(549) and SNAP(649)-eIF3 complexes. View-field is approximately 750 μm^2. Inset shows model of 40S-IRES-ternary complex with labeling positions. (**C**) Single-molecule fluorescence trace of ternary complex containing 40S-SNAP(549), HCV IRES, and SNAP(649)-eIF3. As annotated, steep decreases in fluorescence may indicate either single-molecule photobleaching or dissociation events.

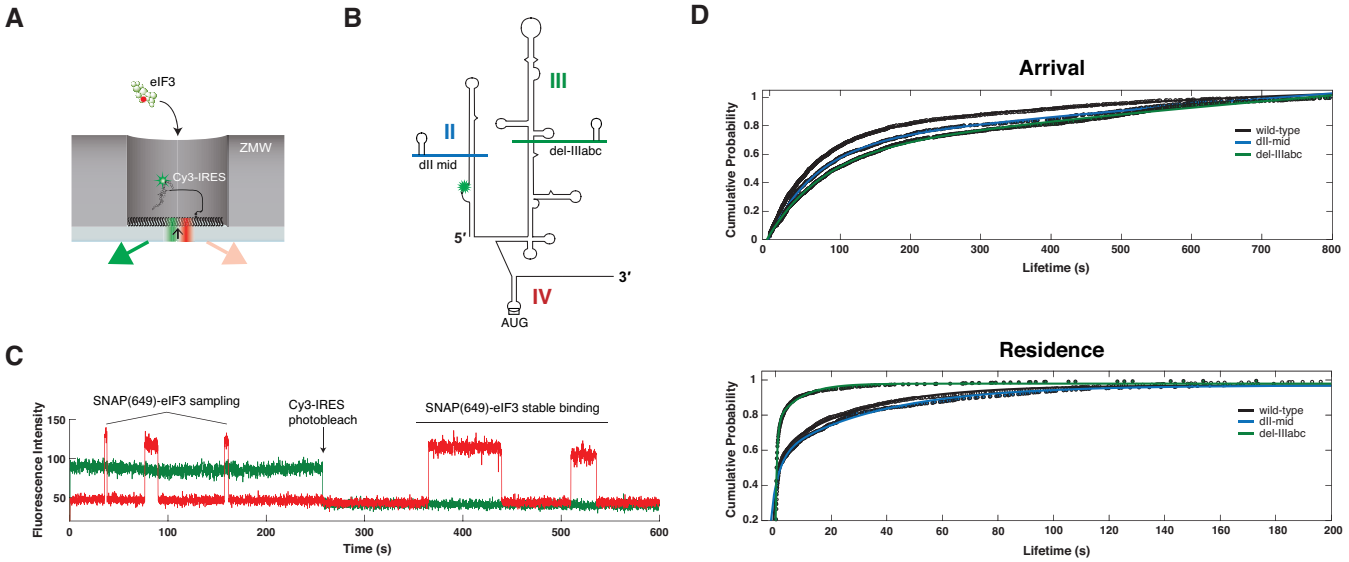

Figure 5. Single molecule analysis of SNAP–eIF3 binding to the HCV IRES RNA in ZMWs. (**A**) ZMW schematic showing immobilized Cy3-IRES RNA and delivery of the SNAP(649)-labeled eIF3. (**B**) Secondary structure cartoon showing wild-type and mutated HCV IRESs. (**C**) Representative single-molecule fluorescence trace showing SNAP–eIF3 arrival and residence on wild-type Cy3-IRES, as bursts of red fluorescence signal, following delivery of 1 nM SNAP–eIF3. The trace is annotated to indicate the Cy3-IRES photobleaching event at ∼250 seconds into acquisition, as well as SNAP(649)-eIF3 sampling and stable binding events. (**D**) Cumulative distribution plots of arrival and residence lifetimes to wild-type and del-IIIabc mutant IRESs, where the fast and slow phases have been fit by a double exponential function. The number of molecules (n) used to calculate lifetimes for fits are 392, 269, and 468 for wild-type, dII-mid, and del-IIIabc IRES RNAs, respectively.

some core components (20,52,55). Subunit-h has been implicated in lens development in zebrafish, re-initiation after upstream open reading frames in *Arabidopsis thaliana* and mammals, and is upregulated in several cancers (59–63). The concurrent loss of subunits of the 'right leg' of the PCI/MPN octamer (k and l) in the eIF3H KO is consistent with a RNAi knockdown study in HeLa cells and the IP results in a previously reported eIF3H KO in HEK293T cells (13,55). The k and l subunits independently form a dimer and are likely destabilized in the absence of eIF3h, as suggested previously, since their mRNA levels are unchanged between wild-type and knockdown cells (13,55).

eIF3h protein levels appear to control cellular growth rate at the level of translation (13,55,62). Our results suggest that eIF3h content is near a threshold in Hap1 cells, since overexpression of SNAP–eIF3H appears to diminish wild-type eIF3h protein levels and fails to increase the proliferation rate of wild-type cells. Like subunits k and l, eIF3h may

be destabilized when not bound in the eIF3 complex and lead to this observed saturation. Alternatively, eIF3h translation may be regulated by a negative-feedback loop, perhaps post-transcriptionally, as it is a terminal oligopyrimidine (TOP) mRNA and contains an eIF3-binding sequence within its open reading frame, which folds into a –16.9 kcal/mol stem loop *in silico* (35,64,65) (Supplemental Figure S6). Growth defects of the eIF3H KO may be partially mediated through the concurrent loss of the k and l subunits; however, independent knockdown of these subunits shows no drastic changes in growth (13). The k and l subunits are likely dispensable for growth in human cells as they are in *Neurospora*, and further appear to be non-essential in *C. elegans*, where their absence increases longevity (53,66).

As with the ribosome, eIF3 compositional heterogeneity may control the translation of specific mRNA transcripts (67,68). We found that eIF3h-deficiency affects the translation of select mRNAs, as the ratio of cap-independent to cap-dependent translation decreased for the EMCV and the PV IRESs, but not for the HCV and the CrPV IGR IRESs (Supplementary Figure S5). This result indicates that the intact eIF3 is not necessary for HCV IRES-mediated translation, despite the conserved interaction of eIF3 with domain III of the IRES. Unlike the HCV and the CrPV IGR IRES, the EMCV and the PV IRESs require components of the eIF4F complex for their function, but only the PV IRES requires a direct eIF3–eIF4G interaction (69,70). Immunoprecipitation experiments have shown that in addition to eIF3k and l, subunits d and e are partially detached from eIF3 in the absence of eIF3h, and both subunits are known to mediate an interaction with eIF4G (55,71). These observations suggest that loss of eIF3h may disrupt an important communication with eIF4F during initiation, which may or may not require a direct eIF3–eIF4G interaction. Although not necessary for translation, eIF3h levels may thus fine tune the stability of modules within the eIF3 complex to coordinate eIF4F position and/or abundance within 43S PICs.

Affinity purification of SNAP–eIF3h yielded a complete eIF3 complex that allows biophysical analysis and recapitulates known *in vitro* binding activity with the HCV IRES and 40S ribosomal subunit, demonstrating that the 'torso' of the PCI/MPN octamer is a non-disruptive position to place the SNAP-tag label (21) (Figure 3). We observed a fluorescent ternary 40S–IRES–eIF3 complex in bulk and at the single-molecule level in a static TIRFM assay, where long-lived complexes remain visible on the surface for minutes (Figure 4). In contrast, the eIF3–IRES binary complex appears as a smear on an acrylamide/agarose composite gel, likely a result of the dynamic nature of this binding interaction.

Our real-time data directly demonstrates the dynamic nature of the eIF3–IRES interaction, wherein SNAP–eIF3 resides on the IRES over a wide distribution of both short and long time events (Figure 5). Given that the HCV IRES is structurally flexible and samples an ensemble of conformations in solution, our data likely includes short, non-productive eIF3 sampling events to RNA conformers in which the IIIabc junction is inaccessible (72). The slight increase in arrival rates to the wild-type versus mutant IRESs might result from differences in RNA folding, wherein the wild-type IRES may sample conformations that better expose RNA structures and increase eIF3 binding probability. Analysis of hundreds of molecules unambiguously shows that eIF3 binding is specific to the apical region of domain III: deletion of the IIIabc junction substantially decreases the dwell-times of eIF3 on the HCV IRES, while deletion of the domain II apical region causes little effect. As with the long-lived complexes in the static single-molecule experiment using TIRFM, dwell times may increase even more in the context of the 40S-IRES–eIF3 ternary complex, potentially resulting from increased avidity provided by contacts of eIF3 peripheral subunits with the 40S ribosomal subunit. Together, our kinetic data indicate that, in a simple model system, eIF3 transiently surveys diverse RNA molecules, and upon recognition of the IIIabc junction, locks onto the RNA for long dwell-times (average lifetime of slow phase at ~30 sec) such that it may further orchestrate multiple activities to facilitate translation initiation from the IRES.

Pathway models of HCV IRES-mediated initiation typically suggest that eIF3, together with the Met-tRNAi^{Met}-eIF2-GTP ternary complex (eIF2-TC), bind to a preformed 40S–IRES complex to form the 48S PIC, and subsequent rearrangements drive formation of an 80S initiation complex (27,29). However, eIF2-TC and eIF3 binding events are unlikely to be simultaneous, and eIF2-independent pathways have been shown to exist (73–75). Given that the HCV IRES and eIF3 compete for a similar binding region on the 40S ribosomal subunit, how the IRES might actively remodel canonical 43S PICs to favor translation of the HCV genome remains an open question (57,76). Our ability to purify and label both ribosomal subunits and human eIF3 is thus a crucial step towards dissecting the kinetic pathways of initiation on type 3 HCV-like IRESs. However, these labelled components must be tracked in fully reconstituted, translationally-active biochemical systems containing additional factors to draw firm mechanistic insights into HCV IRES-mediated translation.

The elucidation of eIF3's function in viral IRES-mediated translation has implications for canonical translation initiation, where some of the principles governing initiation may be shared. The interaction of eIF3 with domain IIIabc of the HCV IRES could be analogous to the interaction of eIF3 with stem-loop structures formed within certain cellular mRNA species, albeit these interactions are not known to drive cap-independent initiation (35,36). Additionally, eIF3 is a proposed 'reader' of N6-methyladensosine (m^{6}A) within cellular RNAs, where it may promote cap-independent translation by direct binding to m^{6}A nucleotides in 5'UTRs and/or translation efficiency through interactions with YTHDF1, another reader of m^{6}A (77,78). Fluorescently-labelled eIF3 could further enable interrogation into how such RNA structures and modifications function in mRNA selection and ribosome loading during initiation.

Our study outlines a generalizable strategy for the affinity-purification and the fluorescent-labelling of a nearly MegaDalton-sized protein complex directly from human cells. Through validation in cells and *in vitro*, we demonstrate that our tagged complex is stable, functional, and specifically interacts with RNA in bulk and in single-molecule assays. The fluorescently-labelled eIF3 will be a

crucial tool for mechanistic investigations into the dynamics of human translation initiation.

SUPPLEMENTARY DATA

Supplementary Data are available at NAR online.

ACKNOWLEDGEMENTS

The authors thank the Sarnow and Carette laboratories for helpful discussions and experimental advice, and Christopher Fraser for advice on HeLa eIF3 purification. We thank Christopher Lapointe for critical reading of the manuscript. The Stanford FACS facility provided assistance with cell sorting.

FUNDING

National Science Foundation Graduate Research Fellowship [DGE-114747 to A.G.J.]; Stanford Bio-X fellowship (to J.C.); National Institute of Health [AI047365, AI099506 to J.D.P.]. Funding for open access charge: National Institute of Health.
Conflict of interest statement. None declared.

REFERENCES

1. Jackson,R.J., Hellen,C.U. and Pestova,T.V. (2010) The mechanism of eukaryotic translation initiation and principles of its regulation. *Nat. Rev. Mol. Cell Biol.*, **11**, 113–127.
2. Sonenberg,N. and Hinnebusch,A.G. (2009) Regulation of translation initiation in eukaryotes: mechanisms and biological targets. *Cell*, **136**, 731–745.
3. Aitken,C.E. and Lorsch,J.R. (2012) A mechanistic overview of translation initiation in eukaryotes. *Nat. Struct. Mol. Biol.*, **19**, 568–576.
4. Hinnebusch,A.G. (2014) The scanning mechanism of eukaryotic translation initiation. *Annu. Rev. Biochem.*, **83**, 779–812.
5. Fraser,C.S. (2015) Quantitative studies of mRNA recruitment to the eukaryotic ribosome. *Biochimie*, **114**, 58–71.
6. Valasek,L.S. (2012) 'Ribozoomin'–translation initiation from the perspective of the ribosome-bound eukaryotic initiation factors (eIFs). *Curr. Protein Pept. Sci.*, **13**, 305–330.
7. Petrov,A. and Puglisi,J.D. (2010) Site-specific labeling of Saccharomyces cerevisiae ribosomes for single-molecule manipulations. *Nucleic Acids Res.*, **38**, e143.
8. Fuchs,G., Petrov,A.N., Marceau,C.D., Popov,L.M., Chen,J., O'Leary,S.E., Wang,R., Carette,J.E., Sarnow,P. and Puglisi,J.D. (2015) Kinetic pathway of 40S ribosomal subunit recruitment to hepatitis C virus internal ribosome entry site. *Proc. Natl. Acad. Sci. U.S.A.*, **112**, 319–325.
9. Petrov,A., Grosely,R., Chen,J., O'Leary,S.E. and Puglisi,J.D. (2016) Multiple parallel pathways of translation initiation on the CrPV IRES. *Mol. Cell*, **62**, 92–103.
10. Hinnebusch,A.G. (2006) eIF3: a versatile scaffold for translation initiation complexes. *Trends Biochem. Sci.*, **31**, 553–562.
11. Zhou,M., Sandercock,A.M., Fraser,C.S., Ridlova,G., Stephens,E., Schenauer,M.R., Yokoi-Fong,T., Barsky,D., Leary,J.A., Hershey,J.W. *et al.* (2008) Mass spectrometry reveals modularity and a complete subunit interaction map of the eukaryotic translation factor eIF3. *Proc. Natl. Acad. Sci. U.S.A.*, **105**, 18139–18144.
12. Cate,J.H. (2017) Human eIF3: from 'blobology' to biological insight. *Philos. Trans. R Soc. Lond. B Biol.Sci.*, **372**, 20160176.
13. Wagner,S., Herrmannova,A., Sikrova,D. and Valasek,L.S. (2016) Human eIF3b and eIF3a serve as the nucleation core for the assembly of eIF3 into two interconnected modules: the yeast-like core and the octamer. *Nucleic Acids Res.*, **44**, 10772–10788.
14. Pisareva,V.P. and Pisarev,A.V. (2016) DHX29 and eIF3 cooperate in ribosomal scanning on structured mRNAs during translation initiation. *RNA*, **22**, 1859–1870.
15. Aitken,C.E., Beznoskova,P., Vlckova,V., Chiu,W.L., Zhou,F., Valasek,L.S., Hinnebusch,A.G. and Lorsch,J.R. (2016) Eukaryotic translation initiation factor 3 plays distinct roles at the mRNA entry and exit channels of the ribosomal preinitiation complex. *Elife*, **5**, e20934.
16. Sharifulin,D.E., Bartuli,Y.S., Meschaninova,M.I., Ven'yaminova,A.G., Graifer,D.M. and Karpova,G.G. (2016) Exploring accessibility of structural elements of the mammalian 40S ribosomal mRNA entry channel at various steps of translation initiation. *Biochim. Biophys. Acta*, **1864**, 1328–1338.
17. Fraser,C.S., Hershey,J.W. and Doudna,J.A. (2009) The pathway of hepatitis C virus mRNA recruitment to the human ribosome. *Nat. Struct. Mol. Biol.*, **16**, 397–404.
18. Fraser,C.S., Berry,K.E., Hershey,J.W. and Doudna,J.A. (2007) eIF3j is located in the decoding center of the human 40S ribosomal subunit. *Mol. Cell*, **26**, 811–819.
19. Pick,E., Hofmann,K. and Glickman,M.H. (2009) PCI complexes: Beyond the proteasome, CSN, and eIF3 Troika. *Mol. Cell*, **35**, 260–264.
20. Sun,C., Todorovic,A., Querol-Audi,J., Bai,Y., Villa,N., Snyder,M., Ashchyan,J., Lewis,C.S., Hartland,A., Gradia,S. *et al.* (2011) Functional reconstitution of human eukaryotic translation initiation factor 3 (eIF3). *Proc. Natl. Acad. Sci. U.S.A.*, **108**, 20473–20478.
21. Hinnebusch,A.G. (2017) Structural insights into the mechanism of scanning and start codon recognition in eukaryotic translation initiation. *Trends Biochem Sci*, **42**, 589-611.
22. Siridechadilok,B., Fraser,C.S., Hall,R.J., Doudna,J.A. and Nogales,E. (2005) Structural roles for human translation factor eIF3 in initiation of protein synthesis. *Science*, **310**, 1513–1515.
23. Querol-Audi,J., Sun,C., Vogan,J.M., Smith,M.D., Gu,Y., Cate,J.H. and Nogales,E. (2013) Architecture of human translation initiation factor 3. *Structure*, **21**, 920–928.
24. des Georges,A., Dhote,V., Kuhn,L., Hellen,C.U., Pestova,T.V., Frank,J. and Hashem,Y. (2015) Structure of mammalian eIF3 in the context of the 43S preinitiation complex. *Nature*, **525**, 491–495.
25. Hashem,Y., des Georges,A., Dhote,V., Langlois,R., Liao,H.Y., Grassucci,R.A., Hellen,C.U., Pestova,T.V. and Frank,J. (2013) Structure of the mammalian ribosomal 43S preinitiation complex bound to the scanning factor DHX29. *Cell*, **153**, 1108–1119.
26. Simonetti,A., Brito Querido,J., Myasnikov,A.G., Mancera-Martinez,E., Renaud,A., Kuhn,L. and Hashem,Y. (2016) eIF3 peripheral subunits rearrangement after mRNA binding and start-codon recognition. *Mol. Cell*, **63**, 206–217.
27. Fraser,C.S. and Doudna,J.A. (2007) Structural and mechanistic insights into hepatitis C viral translation initiation. *Nat. Rev. Microbiol.*, **5**, 29–38.
28. Lukavsky,P.J. (2009) Structure and function of HCV IRES domains. *Virus Res.*, **139**, 166–171.
29. Johnson,A.G., Grosely,R., Petrov,A.N. and Puglisi,J.D. (2017) Dynamics of IRES-mediated translation. *Philos. Trans. R Soc. Lond. B Biol. Sci.*, **372**, 20160177.
30. Kieft,J.S., Zhou,K., Jubin,R. and Doudna,J.A. (2001) Mechanism of ribosome recruitment by hepatitis C IRES RNA. *RNA*, **7**, 194–206.
31. Ji,H., Fraser,C.S., Yu,Y., Leary,J. and Doudna,J.A. (2004) Coordinated assembly of human translation initiation complexes by the hepatitis C virus internal ribosome entry site RNA. *Proc. Natl. Acad. Sci. U.S.A.*, **101**, 16990–16995.
32. Otto,G.A. and Puglisi,J.D. (2004) The pathway of HCV IRES-mediated translation initiation. *Cell*, **119**, 369–380.
33. Sun,C., Querol-Audi,J., Mortimer,S.A., Arias-Palomo,E., Doudna,J.A., Nogales,E. and Cate,J.H. (2013) Two RNA-binding motifs in eIF3 direct HCV IRES-dependent translation. *Nucleic Acids Res.*, **41**, 7512–7521.
34. Asnani,M., Kumar,P. and Hellen,C.U. (2015) Widespread distribution and structural diversity of Type IV IRESs in members of Picornaviridae. *Virology*, **478**, 61–74.
35. Lee,A.S., Kranzusch,P.J. and Cate,J.H. (2015) eIF3 targets cell-proliferation messenger RNAs for translational activation or repression. *Nature*, **522**, 111–114.
36. Lee,A.S., Kranzusch,P.J., Doudna,J.A. and Cate,J.H. (2016) eIF3d is an mRNA cap-binding protein that is required for specialized translation initiation. *Nature*, **536**, 96–99.

37. Ran,F.A., Hsu,P.D., Wright,J., Agarwala,V., Scott,D.A. and Zhang,F. (2013) Genome engineering using the CRISPR-Cas9 system. *Nat. Protoc.*, **8**, 2281–2308.
38. Sowa,M.E., Bennett,E.J., Gygi,S.P. and Harper,J.W. (2009) Defining the human deubiquitinating enzyme interaction landscape. *Cell*, **138**, 389–403.
39. Campeau,E., Ruhl,V.E., Rodier,F., Smith,C.L., Rahmberg,B.L., Fuss,J.O., Campisi,J., Yaswen,P., Cooper,P.K. and Kaufman,P.D. (2009) A versatile viral system for expression and depletion of proteins in mammalian cells. *PLoS One*, **4**, e6529.
40. Damoc,E., Fraser,C.S., Zhou,M., Videler,H., Mayeur,G.L., Hershey,J.W., Doudna,J.A., Robinson,C.V. and Leary,J.A. (2007) Structural characterization of the human eukaryotic initiation factor 3 protein complex by mass spectrometry. *Mol. Cell. Proteomics*, **6**, 1135–1146.
41. Kim,I., Lukavsky,P.J. and Puglisi,J.D. (2002) NMR study of 100 kDa HCV IRES RNA using segmental isotope labeling. *J. Am. Chem. Soc.*, **124**, 9338–9339.
42. Lukavsky,P.J., Kim,I., Otto,G.A. and Puglisi,J.D. (2003) Structure of HCV IRES domain II determined by NMR. *Nat. Struct. Biol.*, **10**, 1033–1038.
43. Quade,N., Boehringer,D., Leibundgut,M., van den Heuvel,J. and Ban,N. (2015) Cryo-EM structure of Hepatitis C virus IRES bound to the human ribosome at 3.9-A resolution. *Nat. Commun.*, **6**, 7646.
44. Yamamoto,H., Collier,M., Loerke,J., Ismer,J., Schmidt,A., Hilal,T., Sprink,T., Yamamoto,K., Mielke,T., Burger,J. *et al.* (2015) Molecular architecture of the ribosome-bound Hepatitis C Virus internal ribosomal entry site RNA. *EMBO J.*, **34**, 3042–3058.
45. Jan,E., Kinzy,T.G. and Sarnow,P. (2003) Divergent tRNA-like element supports initiation, elongation, and termination of protein biosynthesis. *Proc. Natl. Acad. Sci. U.S.A.*, **100**, 15410–15415.
46. Suh,M.H., Ye,P., Datta,A.B., Zhang,M. and Fu,J. (2005) An agarose-acrylamide composite native gel system suitable for separating ultra-large protein complexes. *Anal. Biochem.*, **343**, 166–175.
47. Aitken,C.E., Marshall,R.A. and Puglisi,J.D. (2008) An oxygen scavenging system for improvement of dye stability in single-molecule fluorescence experiments. *Biophys. J.*, **94**, 1826–1835.
48. Chen,J., Dalal,R.V., Petrov,A.N., Tsai,A., O'Leary,S.E., Chapin,K., Cheng,J., Ewan,M., Hsiung,P.L., Lundquist,P. *et al.* (2014) High-throughput platform for real-time monitoring of biological processes by multicolor single-molecule fluorescence. *Proc. Natl. Acad. Sci. U.S.A.*, **111**, 664–669.
49. Valasek,L., Hasek,J., Trachsel,H., Imre,E.M. and Ruis,H. (1999) The Saccharomyces cerevisiae HCR1 gene encoding a homologue of the p35 subunit of human translation initiation factor 3 (eIF3) is a high copy suppressor of a temperature-sensitive mutation in the Rpg1p subunit of yeast eIF3. *J. Biol. Chem.*, **274**, 27567–27572.
50. Ray,A., Bandyopadhyay,A., Matsumoto,T., Deng,H. and Maitra,U. (2008) Fission yeast translation initiation factor 3 subunit eIF3h is not essential for global translation initiation, but deletion of eif3h+ affects spore formation. *Yeast*, **25**, 809–823.
51. Zhou,C., Arslan,F., Wee,S., Krishnan,S., Ivanov,A.R., Oliva,A., Leatherwood,J. and Wolf,D.A. (2005) PCI proteins eIF3e and eIF3m define distinct translation initiation factor 3 complexes. *BMC Biol.*, **3**, 14.
52. Masutani,M., Sonenberg,N., Yokoyama,S. and Imataka,H. (2007) Reconstitution reveals the functional core of mammalian eIF3. *EMBO J.*, **26**, 3373–3383.
53. Smith,M.D., Gu,Y., Querol-Audi,J., Vogan,J.M., Nitido,A. and Cate,J.H. (2013) Human-like eukaryotic translation initiation factor 3 from Neurospora crassa. *PLoS One*, **8**, e78715.
54. Majzoub,K., Hafirassou,M.L., Meignin,C., Goto,A., Marzi,S., Fedorova,A., Verdier,Y., Vinh,J., Hoffmann,J.A., Martin,F. *et al.* (2014) RACK1 controls IRES-mediated translation of viruses. *Cell*, **159**, 1086–1095.
55. Smith,M.D., Arake-Tacca,L., Nitido,A., Montabana,E., Park,A. and Cate,J.H. (2016) Assembly of eIF3 mediated by mutually dependent subunit insertion. *Structure*, **24**, 886–896.
56. Carette,J.E., Raaben,M., Wong,A.C., Herbert,A.S., Obernosterer,G., Mulherkar,N., Kuehne,A.I., Kranzusch,P.J., Griffin,A.M., Ruthel,G. *et al.* (2011) Ebola virus entry requires the cholesterol transporter Niemann-Pick C1. *Nature*, **477**, 340–343.
57. Hashem,Y., des Georges,A., Dhote,V., Langlois,R., Liao,H.Y., Grassucci,R.A., Pestova,T.V., Hellen,C.U. and Frank,J. (2013) Hepatitis-C-virus-like internal ribosome entry sites displace eIF3 to gain access to the 40S subunit. *Nature*, **503**, 539–543.
58. Sizova,D.V., Kolupaeva,V.G., Pestova,T.V., Shatsky,I.N. and Hellen,C.U. (1998) Specific interaction of eukaryotic translation initiation factor 3 with the 5' nontranslated regions of hepatitis C virus and classical swine fever virus RNAs. *J Virol*, **72**, 4775–4782.
59. Choudhuri,A., Maitra,U. and Evans,T. (2013) Translation initiation factor eIF3h targets specific transcripts to polysomes during embryogenesis. *Proc. Natl. Acad. Sci. U.S.A.*, **110**, 9818–9823.
60. Roy,B., Vaughn,J.N., Kim,B.H., Zhou,F., Gilchrist,M.A. and Von Arnim,A.G. (2010) The h subunit of eIF3 promotes reinitiation competence during translation of mRNAs harboring upstream open reading frames. *RNA*, **16**, 748–761.
61. Hershey,J.W. (2015) The role of eIF3 and its individual subunits in cancer. *Biochim. Biophys. Acta*, **1849**, 792–800.
62. Zhang,L., Smit-McBride,Z., Pan,X., Rheinhardt,J. and Hershey,J.W. (2008) An oncogenic role for the phosphorylated h-subunit of human translation initiation factor eIF3. *J. Biol. Chem.*, **283**, 24047–24060.
63. Hronova,V., Mohammad,M.P., Wagner,S., Panek,J., Gunisova,S., Zeman,J., Poncova,K. and Valasek,L.S. (2017) Does eIF3 promote reinitiation after translation of short upstream ORFs also in mammalian cells? *RNA Biol.*, 1–8.
64. Iadevaia,V., Caldarola,S., Tino,E., Amaldi,F. and Loreni,F. (2008) All translation elongation factors and the e, f, and h subunits of translation initiation factor 3 are encoded by 5'-terminal oligopyrimidine (TOP) mRNAs. *RNA*, **14**, 1730–1736.
65. Zuker,M. (2003) Mfold web server for nucleic acid folding and hybridization prediction. *Nucleic Acids Res.*, **31**, 3406–3415.
66. Cattie,D.J., Richardson,C.E., Reddy,K.C., Ness-Cohn,E.M., Droste,R., Thompson,M.K., Gilbert,W.V. and Kim,D.H. (2016) Mutations in nonessential eIF3k and eIF3l genes confer lifespan extension and enhanced resistance to ER stress in Caenorhabditis elegans. *PLoS Genet.*, **12**, e1006326.
67. Xue,S. and Barna,M. (2012) Specialized ribosomes: a new frontier in gene regulation and organismal biology. *Nat. Rev. Mol. Cell Biol.*, **13**, 355–369.
68. Shah,M., Su,D., Scheliga,J.S., Pluskal,T., Boronat,S., Motamedchaboki,K., Campos,A.R., Qi,F., Hidalgo,E., Yanagida,M. *et al.* (2016) A transcript-specific eIF3 complex mediates global translational cntrol of energy metabolism. *Cell Rep.*, **16**, 1891–1902.
69. Lomakin,I.B., Hellen,C.U. and Pestova,T.V. (2000) Physical association of eukaryotic initiation factor 4G (eIF4G) with eIF4A strongly enhances binding of eIF4G to the internal ribosomal entry site of encephalomyocarditis virus and is required for internal initiation of translation. *Mol. Cell. Biol.*, **20**, 6019–6029.
70. Sweeney,T.R., Abaeva,I.S., Pestova,T.V. and Hellen,C.U. (2014) The mechanism of translation initiation on Type 1 picornavirus IRESs. *EMBO J.*, **33**, 76–92.
71. Villa,N., Do,A., Hershey,J.W. and Fraser,C.S. (2013) Human eukaryotic initiation factor 4G (eIF4G) protein binds to eIF3c, -d, and -e to promote mRNA recruitment to the ribosome. *J. Biol. Chem.*, **288**, 32932–32940.
72. Perard,J., Leyrat,C., Baudin,F., Drouet,E. and Jamin,M. (2013) Structure of the full-length HCV IRES in solution. *Nat. Commun.*, **4**, 1612.
73. Locker,N., Easton,L.E. and Lukavsky,P.J. (2007) HCV and CSFV IRES domain II mediate eIF2 release during 80S ribosome assembly. *EMBO J.*, **26**, 795–805.
74. Lancaster,A.M., Jan,E. and Sarnow,P. (2006) Initiation factor-independent translation mediated by the hepatitis C virus internal ribosome entry site. *RNA*, **12**, 894–902.
75. Terenin,I.M., Dmitriev,S.E., Andreev,D.E. and Shatsky,I.N. (2008) Eukaryotic translation initiation machinery can operate in a bacterial-like mode without eIF2. *Nat. Struct. Mol. Biol.*, **15**, 836–841.
76. Jaafar,Z.A., Oguro,A., Nakamura,Y. and Kieft,J.S. (2016) Translation initiation by the hepatitis C virus IRES requires eIF1A and ribosomal complex remodeling. *Elife*, **5**, e21198.
77. Meyer,K.D., Patil,D.P., Zhou,J., Zinoviev,A., Skabkin,M.A., Elemento,O., Pestova,T.V., Qian,S.B. and Jaffrey,S.R. (2015) 5' UTR m(6)A promotes cap-independent translation. *Cell*, **163**, 999–1010.

78. Wang,X., Zhao,B.S., Roundtree,I.A., Lu,Z., Han,D., Ma,H., Weng,X., Chen,K., Shi,H. and He,C. (2015) N(6)-methyladenosine modulates messenger RNA translation efficiency. *Cell*, **161**, 1388–1399.
79. Pettersen,E.F., Goddard,T.D., Huang,C.C., Couch,G.S., Greenblatt,D.M., Meng,E.C. and Ferrin,T.E. (2004) UCSF Chimera—a visualization system for exploratory research and analysis. *J. Comput. Chem.*, **25**, 1605–1612.
80. Berman,H.M., Westbrook,J., Feng,Z., Gilliland,G., Bhat,T.N., Weissig,H., Shindyalov,I.N. and Bourne,P.E. (2000) The Protein Data Bank. *Nucleic Acids Res.*, **28**, 235–242.